Letters

Analysis and Design of Load-Independent ZPA Operation for P/S, PS/S, P/SP, and PS/SP Tank Networks in IPT Applications

Suvendu Samanta and Akshay Kumar Rathore

***Abstract*—The zero-phase-angle (ZPA) operation at inverter output of parallel-compensated inductive power transfer (IPT) topologies is frequently reported to be load dependent. Therefore, either the operating inverter switching frequency or the compensation capacitors are modified dynamically with load variation to reach new ZPA point. This letter proposes a novel design technique of compensation capacitors for several IPT topologies to obtain load-independent ZPA. The proposed method is based on the passive selection of tank network parameters; therefore, it obviates the requirement of dynamic tuning and complexities associated with it. A detailed mathematical analysis is reported, and experimental results obtained from a 1-kW lab-prototype are demonstrated to verify the analysis and performance.**

***Index Terms*—Inductive power transfer (IPT), power electronics, resonance.**

I. Introduction

TO REDUCE power converter volt-amp (VA) rating, the primary- and secondary-side compensation capacitors of inductive power transfer (IPT) are tuned such that inverter output voltage and current lie in phase [1]. The inverter displacement power factor at this operating point is unity, and this is commonly known as zero-phase-angle (ZPA) operation, as shown in Fig. 1. This is significant to ensure least voltage and current rating of the inverter switches and, thus, enabling least conduction power loss and compact size. Also, to realize soft switching of inverter devices, the compensation network is often tuned to make the primary-side inverter operate at ZPA or slightly away to reach zero voltage switching (ZVS) or zero current switching (ZCS) conditions [1], [2]. Since the tuned reactive power is relatively small, the parameters for realizing ZVS and ZCS are close to the parameters designed by the ZPA method.

The ZPA operation of series–series compensated IPT topologies is load independent, whereas for parallel-compensated topologies, it is frequently reported to be load dependent [1]–[7]. In an IPT network, parallel-compensated primary topology

Manuscript received September 6, 2017; revised December 21, 2017; accepted January 10, 2018. Date of publication January 22, 2018; date of current version April 20, 2018. *(Corresponding author: Akshay Kumar Rathore.)*

The authors are with the Department of Electrical and Computer Engineering, Concordia University, Montreal, QC H3G 1M8, Canada (e-mail: s_amanta@encs.concordia.ca; akshay.k.rathore@ieee.org).

Color versions of one or more of the figures in this letter are available online at http://ieeexplore.ieee.org.

Digital Object Identifier 10.1109/TPEL.2018.2794623

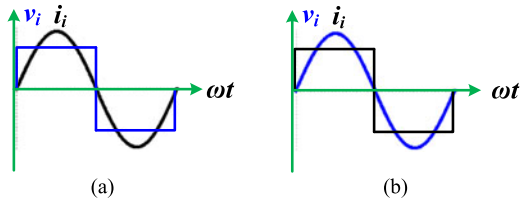

Fig. 1. Ideal inverter output voltage and current profiles at the ZPA operating point: (a) VSI and (b) CSI.

is often reported for several advantages, such as high-quality coil current, lower device current stress, soft switching, and natural short-circuit protection [3], [8]. With parallel compensation in the primary side, the ZPA operation is more desirable because the inverter output voltage is sinusoidal, and the ZPA operation ensures ZVS of inverter switches [9], [10]. The ZPA operation of a parallel-tuned tank fed by a push–pull inverter is reported in [3], [9], and [10]. These are achieved either by dynamically varying tank parameters [9] or by dynamically tuning inverter switching frequency [3], [10]. Along with extra control complexities, the other challenges with the dynamic tuning method include loss of power transfer capability and frequency bifurcation [7]. Therefore, it is always preferred to achieve it through the passive selection of tank capacitors. This will reduce the control effort, which can be focused more on other control goals, viz. meeting load demand, maximum power, efficiency tracking, etc. This letter confirms with a novel design method that parallel-tuned primary tank networks are load independent. The proposed design method is valid for parallel/series (P/S), PS/S, P/SP, and PS/SP tank networks.

II. Proposed Design

The detailed design procedure for deriving load-independent ZPA operating point for IPT topologies with different types of tank circuits are reported here. Fig. 2 shows a PS/S compensated IPT network fed from a full-bridge current source inverter (CSI). The operation of a parallel–series (P/S) tank in primary is like a conventional parallel tank network, but it includes some extra merits, such as higher voltage gain and lower current stress on inverter switches [8]. Fig. 3 shows the transformer equivalent circuit (referred to primary) of the tank network, where leakage (L_{1k}, L_{2k}) and magnetizing impedances (L_m) are related to

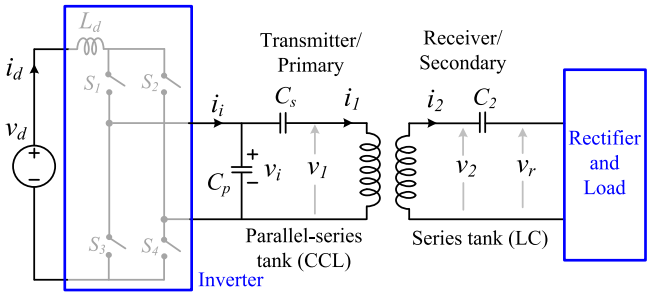

Fig. 2. PS/S compensated IPT network fed from a full bridge CSI.

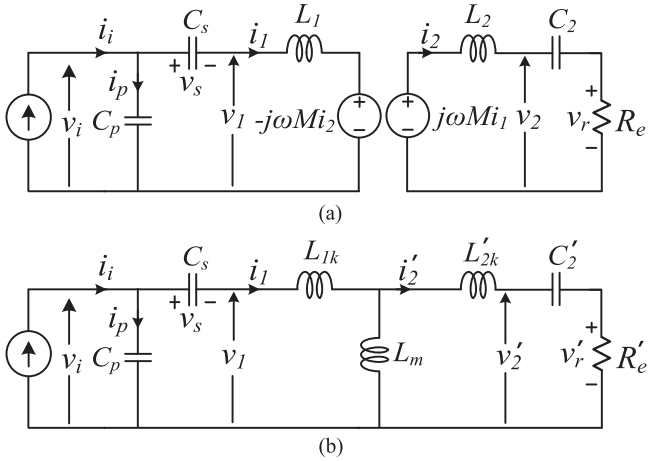

Fig. 3. Transformer equivalent circuit (referred to primary).

their self (L_1, L_2) and mutual inductances (M) as

$$L_{1k} = L_1 - nM \tag{1}$$

$$L_m = nM \tag{2}$$

$$L_{2k} = L_2 - M/n \tag{3}$$

where n is primary to secondary turns ratio. Generally, the usual method of determining the capacitance values for a parallel-tuned IPT circuit with given coil parameters and switching frequency is load dependent. This is explained here briefly.

Because of series compensation at the secondary-side network, the compensation capacitance can be easily set [1], [2], [7] as

$$\omega_o = 1\Big/\sqrt{L_2 C_2} \tag{4}$$

where ω_o is operating frequency or resonance frequency. Therefore, the secondary-side network at resonance frequency becomes resistive. The primary-side capacitance for the ZPA operation is derived using basic network analysis. Using (4), the unity power factor operating point at the output of the primary-side inverter is derived for the P/S resonant tank as

$$C_p = \frac{L_1}{\frac{\omega_o^4 M^4}{{R_e}^2} + \omega_o^2 L_1^2}. \tag{5}$$

For the parallel–series tank (PS/S), this expression is given as

$$C_p = \frac{L_1 - \frac{1}{\omega_o^2 \times C_s}}{\frac{\omega_o^4 M^4}{{R_e}^2} + \omega_o^2 \left(L_1 - \frac{1}{\omega_o^2 \times C_s}\right)^2}. \tag{6}$$

It is clear from both (5) and (6) that the ZPA operation is applicable only for a given load "R_e." The input impedance of the PS/S tank network is plotted for different load impedances, as shown in Fig. 4(a). Clearly, the ZPA operation is possible only for the given load impedance. When load impedance changes, this point drifts significantly. Therefore, dynamic tuning is required to reach the ZPA operating point. However, this plot shows that there exists an operating point that has constant phase angle. If this point is brought to the ZPA line, and the operating frequency is set to that frequency, then the load-independent ZPA operation with these types of topologies is possible. The proposed design method finds out this operating point as follows.

To get a load-independent ZPA operation of this tank network a general impedance analysis is carried out. The input impedance of the network shown in Fig. 3(b) is derived as

$$Z_{\text{in}} = \left\{ Z_1 + j\left(\omega L_{1k} - \frac{1}{\omega C_s}\right)\right\} // \frac{1}{j\omega C_p} = \frac{1}{Y_r + jY_i} \tag{7}$$

where

$$Z_1 = j\omega L_m // \left\{ R_e' + j\left(\omega L_{2k}' - \frac{1}{\omega C_2'}\right)\right\}. \tag{8}$$

The real and complex parts of the admittance are derived as

$$Y_r = \frac{R_e' X_m^2}{t^2 + {R_e'}^2 \{X_m + (X_{1k} - X_s)\}^2} \tag{9}$$

$$\begin{aligned} Y_i = {} & \frac{1}{t^2 + {R_e'}^2 \{X_m + (X_{1k} - X_s)\}^2} \\ & \times [{R_e'}^2 \{X_m + (X_{1k} - X_s)\} \\ & \times [\{X_m + (X_{1k} - X_s)\}/X_p - 1] \\ & - t[X_m - (X_{2k}' - X_2') + t/X_p]] \end{aligned} \tag{10}$$

where the subscripts with every "X" represents impedance of the corresponding element, i.e., $X_m = \omega L_m, X_s = 1/\omega C_s$, etc., and

$$\begin{aligned} t = {} & X_m (X_{2k}' - X_2') + X_m (X_{1k} - X_s) \\ & + (X_{1k} - X_s)(X_{2k}' - X_2'). \end{aligned} \tag{11}$$

From (10), to make the complex part zero, the following conditions must be satisfied, i.e., one of the following expressions has to be zero. Therefore, either

$$\{X_m + (X_{1k} - X_s)\} = 0 \tag{12}$$

$$[\{X_m + (X_{1k} - X_s)\}/X_p - 1] = 0. \tag{13}$$

Out of these two possibilities, the first one leads to $C_p = \infty$; therefore, the only selection is (13). This leads to first condition

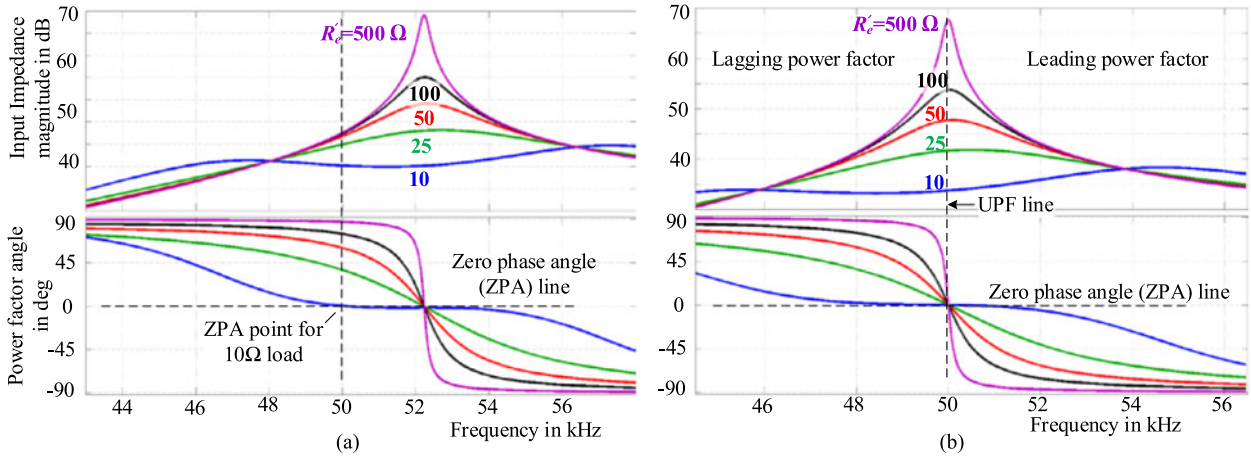

Fig. 4. Input impedance and phase angle variation for a PS/S tank network with (a) existing load-dependent tank design and (b) proposed design.

of load-independent ZPA angle, i.e.,

$$\omega_o = 1\Big/\sqrt{L_1\left(\frac{C_pC_s}{C_p+C_s}\right)}. \tag{14}$$

To achieve load-independent ZPA, the second part of (10) must be zero, i.e., one of the following expressions has to be zero

$$[X_m - (X'_{2k} - X'_2) + t/X_p] = 0 \tag{15}$$

$$t = 0. \tag{16}$$

If (15) is considered, then the required value of C_2 becomes zero. Therefore, the proper selection is $t = 0$, and this leads to the second condition for achieving load-independent ZPA, i.e.,

$$(X'_{2k} - X'_2) = \frac{X_m\,(X_{1k} - X_s)}{X_m + (X_{1k} - X_s)}. \tag{17}$$

The required value of C_2 is calculated from (17) instead of (4). If the tank network components are designed based on (14) and (17), then the ZPA operation at inverter output is always achieved irrespective of any load. In the existing load-dependent ZPA design technique, the secondary-side compensation is simply $X'_2 = X'_{2k} + X_m$. However, in the proposed design, the value of secondary-side compensation is slightly dependent on primary-side coil parameter. This enables to reflect some amount of reactive power from secondary to primary coil to compensate the inverter output power factor due to load deviation. This enables to maintain unity power factor at inverter output irrespective of load change, thereby ensuring lower VA loading on the inverter.

Table I lists the expressions for achieving a load-independent ZPA operation for different combinations of commonly use parallel-compensated IPT tank networks. Similar impedance analysis approach is used for P/SP and PS/SP tank networks to determine the load-independent ZPA operating point. In the complex part of the input impedance for these topologies also have two design constrains. The first constrain determines the transmitter-side compensation capacitances, as listed in Table II. However, the expression for determining the secondary-side capacitances includes load impedance. Therefore, an approximation $R_e >> X_2$ is required to make the resonant tank

TABLE I
DESIGN EXPRESSIONS FOR A LOAD-INDEPENDENT ZPA OPERATION

Tank	Conditions for Load independent ZPA
P/S 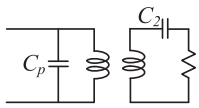	$\omega_o = 1\Big/\sqrt{L_1C_p}$; $(X'_{2k} - X'_2) = \frac{X_mX_{1k}}{X_m+X_{1k}}$ Approximations: no approximations, these are the only conditions for load independent ZPA
PS/S 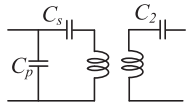	$\omega_o = \frac{1}{\sqrt{L_1(\frac{C_pC_s}{C_p+C_s})}}$; $(X'_{2k} - X'_2) = \frac{X_m(X_{1k}-X_s)}{X_m+(X_{1k}-X_s)}$ Approximations: no approximations, these are the only conditions for load independent ZPA
P/SP 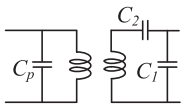	$\omega_o = 1\Big/\sqrt{L_1C_p}$; $(X'_{2k} - X'_1//X'_2) = \frac{X_mX_{1k}}{X_m+X_{1k}}$ Approximations: R_e>>X_2
PS/SP 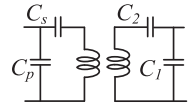	$\omega_o = \frac{1}{\sqrt{L_1(\frac{C_pC_s}{C_p+C_s})}}$; $(X'_{2k} - X'_1//X'_2) = \frac{X_mX_{1k}}{X_m+X_{1k}}$ Approximations: R_e>>X_2

TABLE II
CIRCUIT PARAMETERS FOR A PS/S TANK

Parameters	Selected Values
Switching frequency	50 kHz
TC coil inductance, L_1	131.8 μH
RC coil inductance, L_2	138.4 μH
Mutual inductance, M	30 μH
Tank capacitors, C_p, C_s, C_2	153.8 nF, 153.8 nF, 81.2 nF

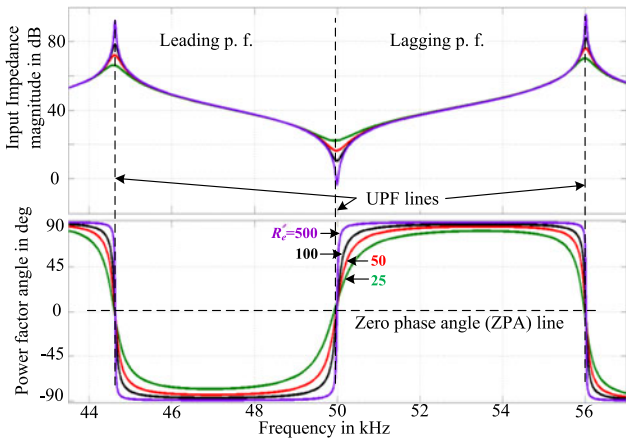

Fig. 5. Input impedance and phase angle variation for a P/SP tank network.

load independent, and corresponding expressions for secondary-side compensation parameter values are given in Table II. Clearly, because of no extra constrains for P/S and PS/S tank networks, this proposed load-independent ZPA operation is more advantageous for these topologies.

Using a circular pad parameter listed in Table II, the required values of the compensation capacitors of the PS/S network are calculated using (14) and (17). For derivation of C_p and C_s, there is only one constrain given in (14). Therefore, there are several combinations of C_p and C_s possible for achieving a load-independent ZPA operation. From [8], higher value of C_p, i.e., lower value of C_s, leads to higher tank gain. Fig. 4 shows the plot of input impedance ($|Z_{\text{in}}|$) and phase $\angle Z_{\text{in}}$ with change in operating frequency. With these proper selections of network components, the ZPA operating point is a fixed point even with wide variation in load. Fig. 5 shows the same impedance plot for the P/SP network with the same IPT coil parameters as the PS/S network. The value of $C_p = 77$ nF, $C_1 = 770.1$ nF, and $C_2 = 85.6$ nF. From Table I and Fig. 5, a parallel tank in secondary imposes one extra constraint for a load-independent ZPA operation. Also, the area around the operating point is quite sharp. This ZPA operating point with parallel-tuned secondary network is very sensitive with parameter variations. Therefore, from practical point of view this design is preferred for series secondary tank.

In view of this proposed load-independent tank design, some important aspects of the ZPA operation of SS and *LCL* topologies are discussed. In the primary side, most commonly used tanks are series [1] and *LCL* topology [11]–[13]. In an *LCL* tank, sometimes an extra capacitor is added in series with the coil to improve the performance. This tank is generally called as *LCLC* tank [14]. The determination of the ZPA operation with all these topologies follows similar the impedance analysis method. However, the derivation of the load-independent ZPA point for series, *LCL,* or *LCLC* topologies is much simpler due to their specific configurations. Also, another merit of these topologies is that a simple voltage source inverter (VSI) can be used to drive these tanks. However, there are some demerits reported in the literature of operating these topologies at the ZPA point. The series-compensated primary faces severe instability issues at light load or in the absence of the secondary circuit [15]. Yao *et.al.* [16] report that the VSI output current with an *LCL* tank contains significant amount of lower order harmonics (third, fifth, seventh, etc.) and they have 90° phase differences from their respective harmonic voltages—i.e., third harmonic current and voltage has 90° phase difference. Although the fundamental component voltage and current are in the same phase, significant harmonic content in current deviates the ZPA operation significantly. Therefore, the ZPA operation with these topologies is not as significant as the parallel-compensated primary topology.

III. Results and Discussions

A. Simulation Results

To verify the proposed load-independent design technique, simulation and experimental results are reported for P/S and PS/S topologies. Figs. 6 and 7 show the simulation results for P/S and PS/S resonant tanks, respectively. The compensation circuit parameters for a P/S tank are $C_p = 77$ nF, and $C_2 = 81.2$ nF, whereas for a PS/S tank, these are listed in Table II. The input voltage for both the cases is 300 V, and rated power output is 1 kW and 250 W, respectively. To verify the performance, the load impedance is varied from 21 and 41 Ω for both the cases. The zoomed views, prior to the load change, during the transient and after settling show that the inverter output voltage and current remain in the same phase for both the topologies. The zoomed view of primary and secondary coil voltages and currents shows the performance of the system at different instants.

B. Experimental Results

To verify the proposed design, a 1-kw experimental porotype is developed where the IPT coils are circular type. Fig. 8 shows the major parts of the experimental setup for a PS/S tank, and component ratings are listed in Table II. Figs. 9 and 10 show the experimental results for 1 kW and 550 W power output when load resistances are 21 Ω and 41 Ω, respectively. It is clear from Figs. 9(a) and 10(a) that irrespective of change in load, the proposed design is maintaining the ZPA operation. Therefore, an inverter needs to supply the least amount of VA for a given load power. This fixed frequency operation is very convenient, whereas variable frequency operation involves complex circuitry and detection of frequency bifurcation, etc. Also, with this parallel-compensated primary, the voltage at the inverter output is sinusoidal, and this voltage directly appears across the inverter switches. Therefore, this unity power factor or ZPA operation directly ensures ZVS turn-on and turn-off of inverter switches.

Figs. 9(b) and 10(b) show the coil voltage and current profiles. These results show that parallel tank in primary side ensures high quality voltage and current profiles. This is because the parallel capacitor (C_p) provides much lower impedance to higher order harmonic currents compare with the coil impedance. Figs. 9(c)

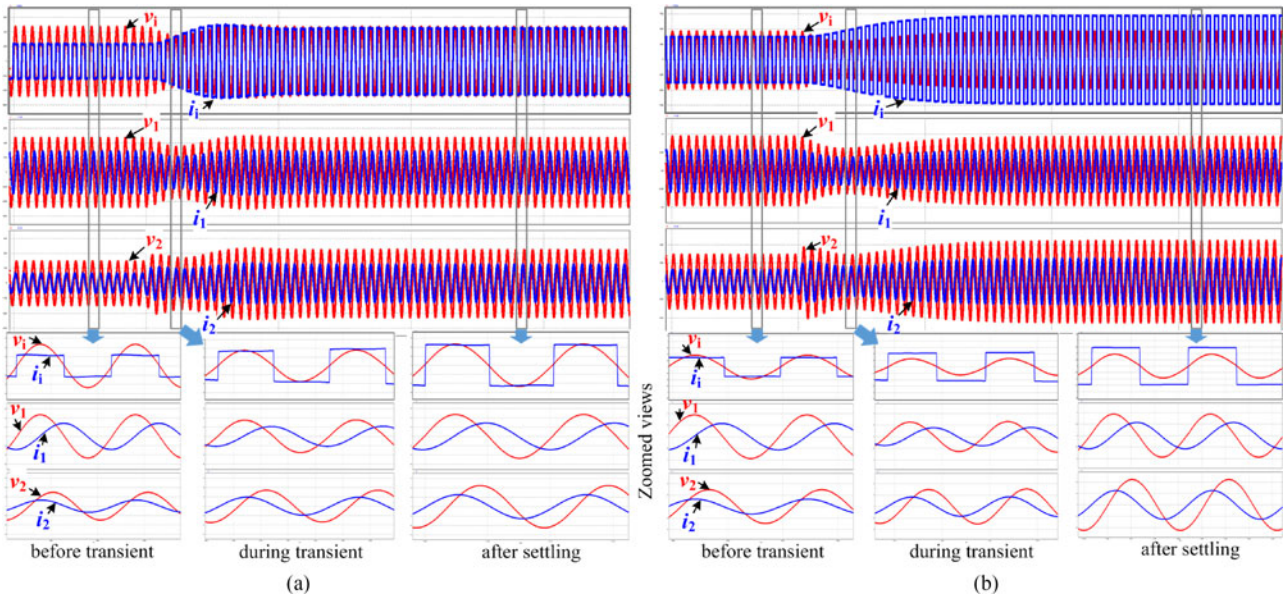

Fig. 6. ZPA operation of a P/S tank: v_i (200 V/div), i_i (1 A/div), v_1 (200 V/div), i_1 (8 A/div), v_2 (100 V/div), and i_2 (4 A/div).

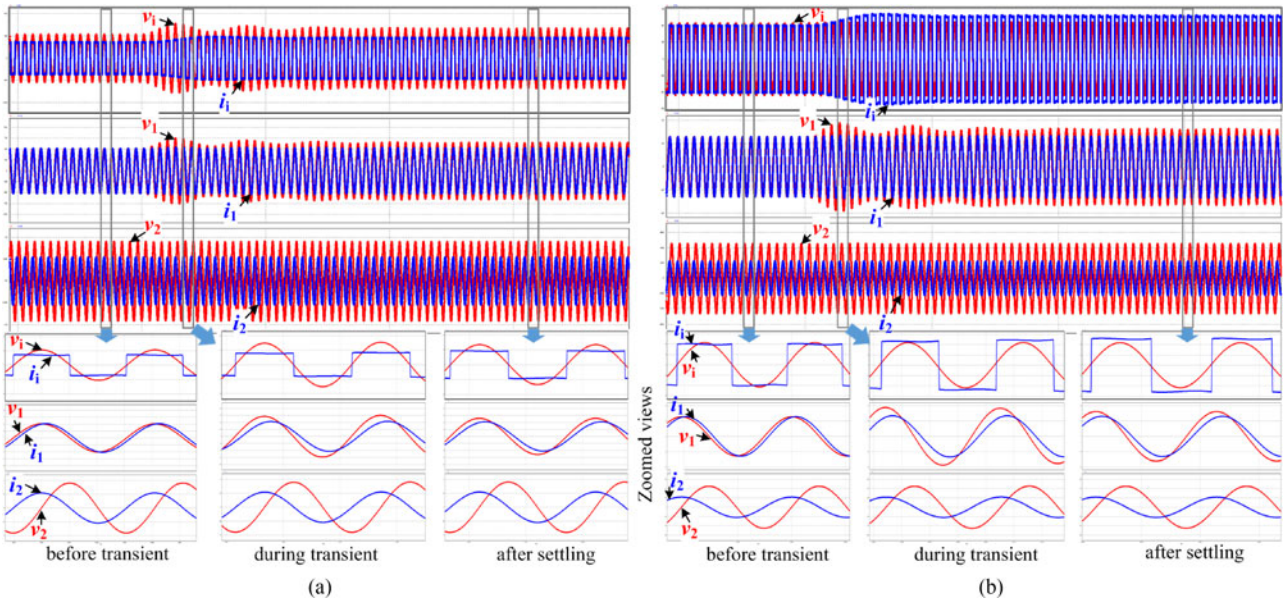

Fig. 7. ZPA operation of a PS/S tank: v_i (250 V/div), i_i (1.25 A/div), v_1 (500 V/div), i_1 (20 A/div), v_2 (200 V/div), and i_2 (8 A/div).

and 10(c) show the voltages across primary-side tank network elements. These results show that parallel–series primary is advantageous compare with only parallel compensation in terms of inverter switch voltage stress. Without capacitor C_s, the inverter output voltage (v_i) is same as coil voltage (v_1), whereas with C_s, v_i is a fraction of v_1.

Fig. 11 verifies the proposed load-independent ZPA operation when there is an input disturbance. The dc-link voltage of the inverter is reduced from rated value, i.e., 300 V to 0 in 500 ms. The zoomed waveforms of these results clearly show that that the resonant tank is capable to operate at ZPA during this wide input disturbance.

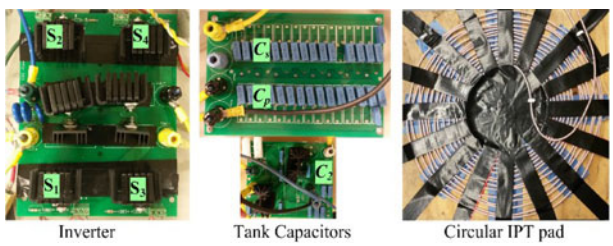

Fig. 8. Experimental setup.

Figs. 12 and 13 show experimental results at full load and half-load when a stiff dc voltage load is connected after the rectifier.

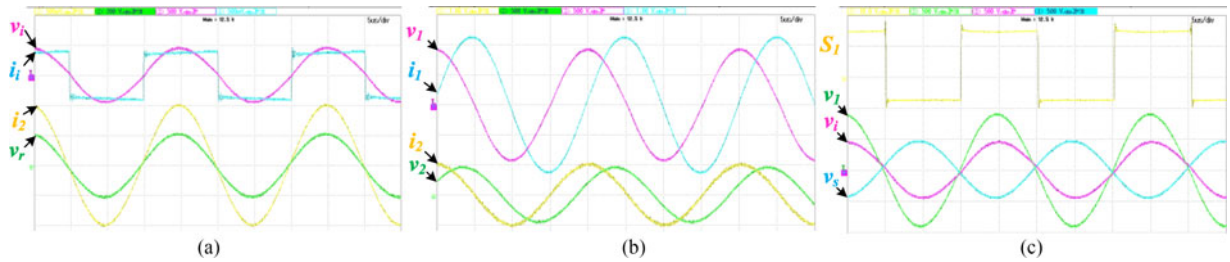

Fig. 9. ZPA operation at 50 kHz, $R = 21\ \Omega$, and $P_o = 1$ kW: (a) inverter output voltage (500 V/div), current (5 A/div), load voltage (200 V/div), and current (5 A/div); (b) primary and secondary coil voltages (500 V/div) and currents (10 A/div); and (c) gating signal of S_1 and voltages across primary-side tank network elements (500 V/div).

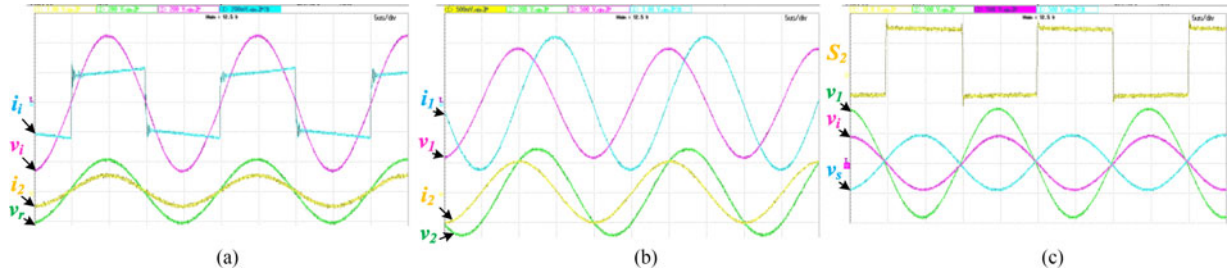

Fig. 10. ZPA operation at 50 kHz, $R = 41\ \Omega$, and $P_o = 550$ W: (a) inverter output voltage (200 V/div), current (2 A/div), load voltage (200 V/div), and current (10 A/div); (b) primary coil voltage (500 V/div) and current (10 A/div) and secondary coil voltage (200 V/div) and current (5 A/div); (c) gating signal of S_2 and voltages across primary-side tank network elements (500 V/div).

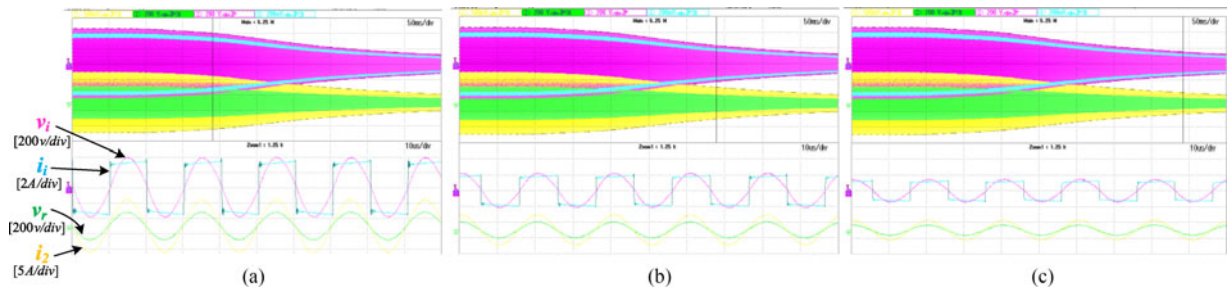

Fig. 11. Verification of a ZPA operation with input disturbance when input dc-link voltage v_d is reduced from rated value (300 V) to zero.

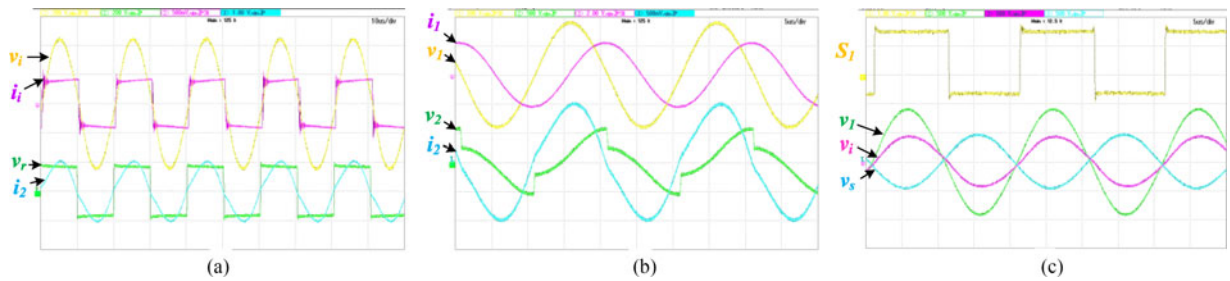

Fig. 12. ZPA operation at 50 kHz, $V_o = 175$ V $P_o = 1$ kW: (a) inverter output voltage (200 V/div), current (5 A/div), load voltage (200 V/div), and current (10 A/div); (b) primary coil voltage (500 V/div) and current (20 A/div) and secondary coil voltage (500 V/div) and current (5 A/div); and (c) gating signal of S_2 and voltages across primary-side tank network elements (500 V/div).

This is like a battery connected at the rectifier output. These results further verify that the proposed design for achieving ZPA is highly insensitive to load change. Fig. 14 shows the performance of the converter when source voltage is varied from half of the rated to rated voltage within 50 ms. The zoomed view of the results before, during, and after the disturbance shows that an inverter operates always at unity displacement power factor. Therefore, an inverter mainly supplies the real power, and it ensures least voltage and current rating of the devices. Along with lowest conduction loss, ZVS turn-on and turn-off of all the inverter and rectifier devices confirm high efficiency and compact size.

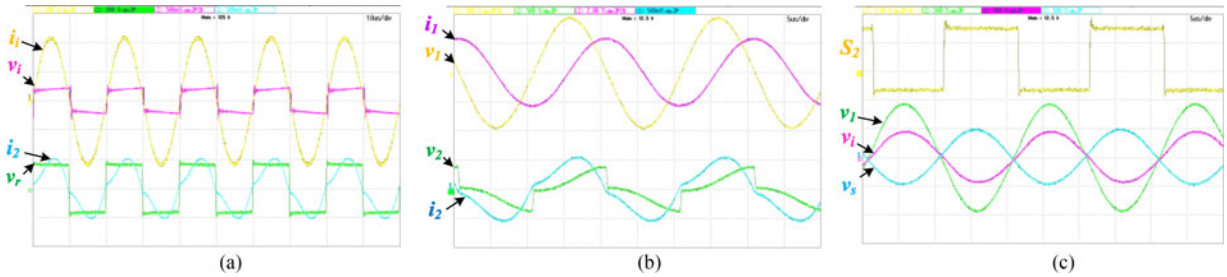

Fig. 13. ZPA operation at 50 kHz, $V_o = 175$ V$P_o = 500$ W: (a) inverter output voltage (200 V/div), current (5 A/div), load voltage (200 V/div), and current (5 A/div); (b) primary coil voltage (500 V/div) and current (20 A/div) and secondary coil voltage (500 V/div) and current (5 A/div); (c) gating signal of S_2 and voltages across primary-side tank network elements (500 V/div).

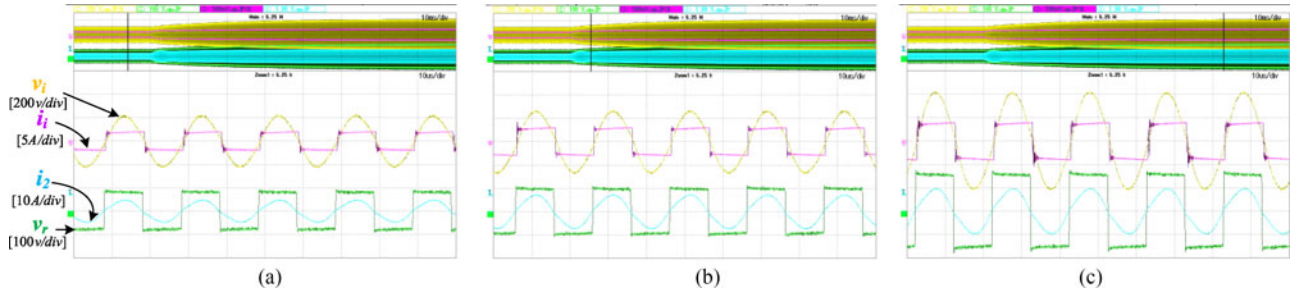

Fig. 14. Verification of a ZPA operation with input disturbance when input dc-link voltage v_d is reduced from rated value (300 V) to half.

IV. Conclusion

This letter reports a novel design method for achieving a load-independent ZPA operation at inverter output for different combinations of IPT topologies. Generally, with parallel compensation this ZPA operation is known to be load dependent. Therefore, to maintain this operation, either variable switching frequency or variable capacitances through switched capacitor are being adopted. However, the proposed design with the passive selection of components enables fixed frequency operation, and it is effective. Therefore, it eliminates frequency bifurcation issues and complexities associated with dynamic tuning. This ZPA operation is very significant to ensure least VA delivered from the inverter, thus enabling lower stress on inverter circuit. Also, this operation is always desirable to achieve ZVS of inverter switches. The proposed analysis and design are verified through experimental results obtained from a 1-kW lab prototype.

References

[1] S. Li and C. Mi, "Wireless power transfer for electric vehicle applications," *IEEE J. Emerg. Sel. Topics Power Electron.*, vol. 3, no. 1, pp. 4–17, Mar. 2015.

[2] J. Sallan, J. L. Villa, A. Llombart, and J. F. Sanz, "Optimal design of ICPT systems applied to electric vehicle battery charge," *IEEE Trans. Ind. Electron.*, vol. 56, no. 6, pp. 2140–2149, Jun. 2009.

[3] G. A. Covic and J. T. Boys, "Inductive power transfer," *Proc. IEEE*, vol. 101, no. 6, pp. 1276–1289, Jun. 2013.

[4] K. Colak, E. Asa, M. Bojarski, D. Czarkowski, and O. C. Onar, "A novel phase-shift control of semibridgeless active rectifier for wireless power transfer," *IEEE Trans. Power Electron.*, vol. 30, no. 11, pp. 6288–6297, Nov. 2015.

[5] G. Buja, M. Bertoluzzo, and K. N. Mude, "Design and experimentation of WPT charger for electric city car," *IEEE Trans. Ind. Electron.*, vol. 62, no. 12, pp. 7436–7447, Dec. 2015.

[6] A. Khaligh and S. Dusmez, "Comprehensive topological analysis of conductive and inductive charging solutions for plug-in electric vehicles," *IEEE Trans. Veh. Technol.*, vol. 61, no. 8, pp. 3475–3489, Oct. 2012.

[7] C. Wang, O. H. Stielau, and G. A. Covic, "Design considerations for a contactless electric vehicle battery charger," *IEEE Trans. Ind. Electron.*, vol. 52, no. 5, pp. 1308–1314, Oct. 2005.

[8] S. Samanta and A. K. Rathore, "Analysis and design of current-fed half-bridge (C)(LC)–(LC) resonant topology for inductive wireless power transfer application," *IEEE Trans. Ind. Appl.*, vol. 53, no. 4, pp. 3917–3926, Jul. 2017.

[9] A. Kamineni, G. A. Covic, and J. T. Boys, "Self-tuning power supply for inductive charging," *IEEE Trans. Power Electron.*, vol. 32, no. 5, pp. 3467–3479, May 2017.

[10] A. P. Hu, G. A. Covic, and J. T. Boys, "Direct ZVS start-up of a current-fed resonant inverter," *IEEE Trans. Power Electron.*, vol. 21, no. 3, pp. 809–812, May 2006.

[11] H. Hao, G. A. Covic, and J. T. Boys, "An approximate dynamic model of LCL- T-based inductive power transfer power supplies," *IEEE Trans. Power Electron.*, vol. 29, no. 10, pp. 5554–5567, Oct. 2014.

[12] H. Hao, G. Covic, and J. Boys, "A parallel topology for inductive power transfer power supplies," *IEEE Trans. Power Electron.*, vol. 29, no. 3, pp. 1140–1151, Mar. 2014.

[13] U. K. Madawala and D. J. Thrimawithana, "A bidirectional inductive power interface for electric vehicles in V2G systems," *IEEE Trans. Ind. Electron.*, vol. 58, no. 10, pp. 4789–4796, Oct. 2011.

[14] S. Weerasinghe, U. K. Madawala, and D. J. Thrimawithana, "A matrix converter-based bidirectional contactless grid interface," *IEEE Trans. Power Electron.*, vol. 32, no. 3, pp. 1755–1766, Mar.2017.

[15] C. Liu, S. Ge, Y. Guo, H. Li, and G. Cai, "Double-LCL resonant compensation network for electric vehicles wireless power transfer: Experimental study and analysis," *IET Power Electron.*, vol. 9, no. 11, pp. 2262–2270, Sep. 2016.

[16] Y. Yao, Y. Wang, X. Liu, F. Lin, and D. G. Xu, "A Novel Parameter Tuning Method for Double-sided LCL Compensated WPT System with Better Comprehensive Performance," *IEEE Trans. Power Electron.*, vol. PP, no. 99, pp. 1–1, doi: 10.1109/TPEL.2017.277825.